Powder Technology 362 (2020) 307–322

Contents lists available at ScienceDirect

Powder Technology

journal homepage: www.elsevier.com/locate/powtec

The effect of temperature on the minimum fluidization conditions of industrial cohesive particles

Roberto Chirone [a], Massimo Poletto [b], Diego Barletta [b], Paola Lettieri [a,*]

[a] Department of Chemical Engineering, University College London, London WC1E 7JE, UK
[b] Dipartimento di Ingegneria Industriale, Università degli Studi di Salerno, Via Giovanni Paolo II, 132, I-84084 Fisciano (SA), Italy

ARTICLE INFO

Article history:
Received 28 November 2018
Received in revised form 13 September 2019
Accepted 25 November 2019
Available online 29 November 2019

ABSTRACT

In order to understand the factors responsible for changes in the fluidization behaviour of industrial particles at high temperatures, an experimental campaign was performed using a 140 × 1000 mm heated gas fluidized bed. Five powder cuts sieved out of the same mother powder covering Group B, A and C of Geldart's classification were investigated over a range of temperatures from ambient to 500 °C. The results show that the mean size distribution affects significantly the fluidization behaviour of the materials investigated. In particular, significant differences were observed in the fluidization behaviour of the coarsest samples (Group B-A) and finest samples (Group A-C). The minimum fluidization conditions were compared with the prediction of the Ergun equation. The comparison was satisfactory only when accounting for the experimental values of the bed voidage. In fact, the non-monotonic trend of the minim velocity for fluidization with increasing temperature cannot be explained only with the effects of temperature on the bed fluid dynamics. But several others are the observed effects on the fluidization behaviour due to the temperature rise that can be ascribed to the enhanced interparticle forces: 1) the increase of the peak of pressure drops, close to the minimum for fluidization, in the fluidization curve at increasing gas velocities; 2) the increase for the finest samples of the hysteresis in the fluidization curves, considering the fluidization and defluidization branches of the curve; 3) a greater tendency of the bed to expand homogeneously; 4) the increasing difference between the parameters of the Richardson-Zaki equation found with a fitting procedure on the experiments and those found using the Richardson-Zaki correlations and the theoretical terminal velocity. Furthermore, in the cases where larger interparticle forces were expected, the X-Ray facility allowed to identify different internal structures within the bed. Mostly vertical channels but also, in the case of the finest powder tested, horizontal channels.

1. Introduction

Fluidization is one of the most used processes involving granular material. It is a common knowledge that fluid-particle processes are largely governed by the forces acting on individual particles [1–10]. The existence of solid-solid interparticle forces such as van der Waals forces, capillary forces and electrostatic forces may explain the non-ideal behavior of fine powders during fluidization. These forces generate links between the particles of the bed, making their free movement difficult and causing a poor fluidization state. It should be noted that solid-solid interaction forces are always present, but they play a different role depending on the relative importance between gravitational and hydrodynamic forces [2,11–13]. In most cases the operating conditions (temperature and pressure) of industrial fluidized bed reactors are far from ambient values [1]. Design criteria and performance predictions for fluidized bed units working at high temperature have been largely based on fluid-dynamic models and correlations established from tests developed at ambient temperature. Generally, the influence of the working temperature on the dynamic features of the system has been considered by simply accounting for the changes of the gas properties, specifically its viscosity and density. However, extrapolating the results and relationships available at ambient conditions to elevated temperatures can lead to misleading predictions of the fluidized bed performance at high temperature. Drastic changes can occur in the fluidization behaviour between low and high temperatures, due to possible modifications induced by the temperature in the structure of the bed. In order to understand the factors responsible for such changes in fluidization behaviour, the role of the interparticles forces (IPFs) and hydrodynamic forces (HDFs) has been studied, but much controversy still remains to define their relative importance. Although several studies have been carried out on the influence of operating conditions on fluidization, the findings are still controversial and a satisfactory understanding of the phenomena which cause differences between ambient and high temperature conditions has not yet been achieved [2,4,6,8,14–22]. In addition, it must

* Corresponding author.
E-mail address: p.lettieri@ucl.ac.uk (P. Lettieri).

https://doi.org/10.1016/j.powtec.2019.11.102
0032-5910/

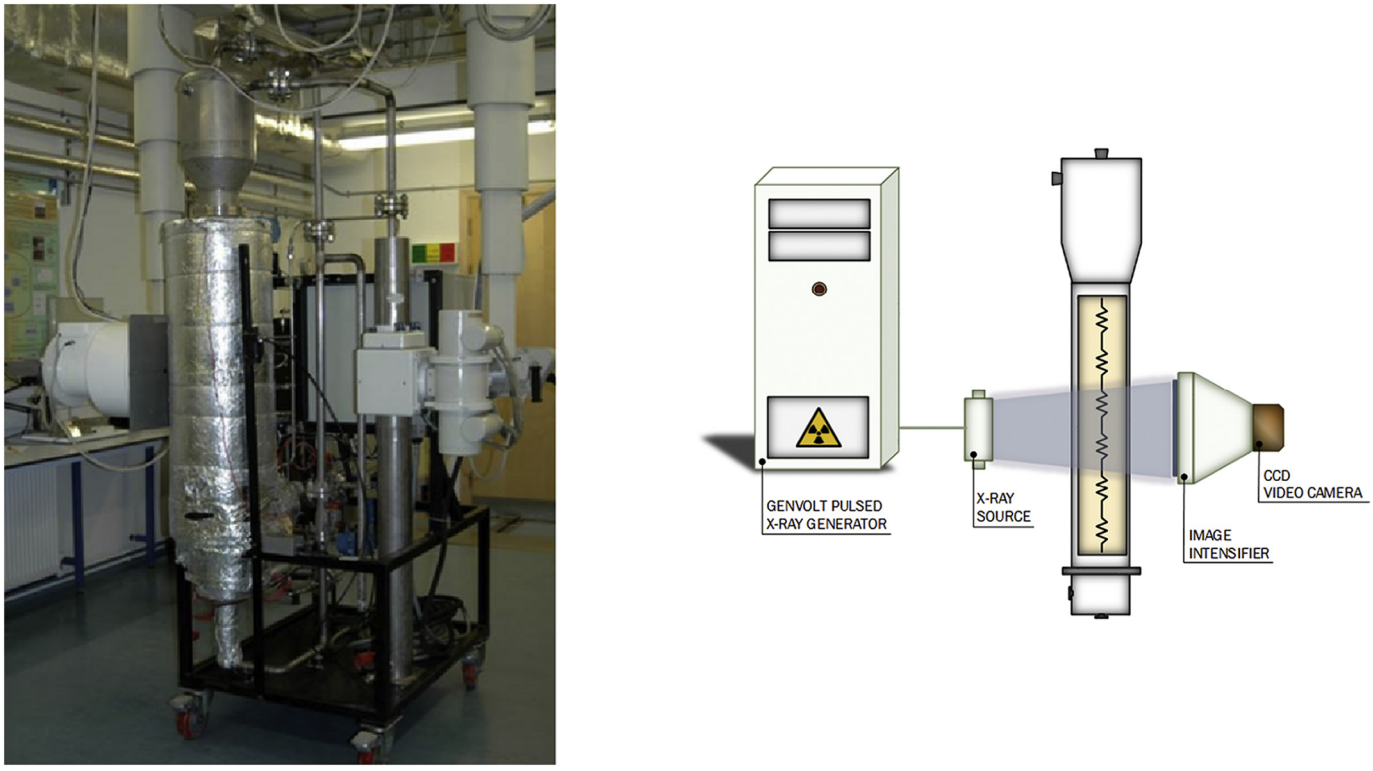

Fig. 1. Experimental apparatus and schematic of the X-ray Imaging technique [36].

be considered that in the case of high temperature processes, the intensity of interparticle cohesive forces, such as capillary, electrostatic and van der Waals forces, can be different from ambient values. These changes are principally due to the variations of particles hardness, the formation of liquid bridge and the modification of the particle dielectric properties [4,23]. Crucial parameters for describing and designing a fluidized bed system are the minimum fluidization velocity and the bed voidage. Several authors studied the dependence on the process temperature of the parameters that characterize the fluidization quality of Geldart A, B and C particles [4,6,11,14,21,24–32]. A non-unique temperature dependency on these parameters was found leading to the conclusion that the temperature effect is the product of the combined variation of both gas properties and dense phase properties with temperature.

The main objective of this work is to provide a basis for the understanding the factors responsible for changes in the fluidization behaviour of industrial cohesive powders. On this purpose, the results of an experimental campaign dealing with the influence of process temperature on the minimum fluidization condition and the bed expansion profiles are presented and where possible results are compared with previous finding on the effect of temperature on the powder flow properties [33].

2. Experimental

2.1. Apparatus

The experimental apparatus used for the experimental campaign is shown in Fig. 1. The fluidized bed reactor is 3 mm thick and it is made in Inconel. The vessel ID is 140 mm and its height is 1000 mm. The vessel is fitted with a very fine (i.e. pore size of 40 μm) Hastelloy X distributor plate to ensure high pressure drops for uniform fluidization. The windbox, below the distributor plate, is made in Inconel. The windbox height is 150 mm and it was packed with 10 mm ceramic balls in order to improve the temperature uniformity. In order to achieve the desired operating temperature, the vessel is surrounded by two flexible ceramic heaters wrapped around the vessel, and capable of providing an operating temperature up to 900 °C. The two ceramic heaters covered 900 mm of the vessel height. To minimize heat losses and for safety reasons, the whole system was packed with two layers of 1.5 cm thick Super-wool, covered by a 7 cm thick layer of Rockwoll wrapped with silver tape. A pressure tap is located above the distribution plate to measure the pressure drop across the bed as a function of the fluidizing gas velocity. Seven thermocouples were used to monitoring and controlling the temperature in the fluidized bed system. The temperature was controlled by three different PID controllers. The set temperatures in the experiments were 25, 100, 200, 300, 400 and 500 °C. The experimental apparatus was equipped with an X-ray facility, available in the Department of Chemical Engineering at University College. It is a non-intrusive tool which allows qualitative and quantitative real-time information on the internal structure and on instantaneous changes in three dimensional systems. Further details are reported by Lettieri and Yates [34]. The X-ray unit consists of a generator, an X-ray source and an image intensifier, as shown in Fig. 1. The X-ray source, or tube, and image intensifier are mounted on a twin column ceiling suspension unit. The two columns can be moved laterally and vertically allowing to change and adjust both the distance between the tube and the image intensifier and the height from the ground of the X-ray beam. All the system is motorized and can be remotely controlled from outside the room. The X-ray generation system provides X-ray pulses of variable width, down to 200 μs, with an intensity up to 450 mA at voltage variable in the range between 50 kV and 150 kV. The X-rays are detected on a 300 mm Industrial X-ray Image Intensifier, optically coupled to a 1024 × 1024 pixel high speed digital CCD camera. The camera is triggered by the control software, which itself is triggered by the X-ray generator at frame rates from 24 to 72 frames per second (fps). All X-ray operations are monitored and controlled from the main control console located outside the radiation proof room, hosting the experimental apparatus. The images are captured, displayed and stored using a powerful image acquisition

software (SPS "iX-Control"). The software handles image processing, image corrections, lossless image storage and playback up to 72 fps in either real-time or frame by frame [34].

2.2. Materials

The experimental campaign was performed on ceramic powders provided by an industrial partner and described elsewhere [33]. In particular, the materials tested is obtained from the virgin material used in a fluidized bed reactor by sieving it in different samples. A small representative amount of each sample was used for characterization analyses, such as those for particle size distribution, shape and chemical composition. In addition, also thermal analyses, such as Thermogravimetric analysis (TGA) and Differential thermal analysis (DTA), were performed.

The physical properties of all materials prior to experiments are reported in Table 1. Results are reported in term of particle size distribution, relative diameter spread and Geldart classification. The samples span from Group B to Group C with particle density of 2330 kg/m^3 at ambient condition. The SEM images (Fig. 2 [33]), show some similar features for all the size cuts analysed. In particular, it can be observed that large quantities of fines adhere on the surface of larger particles that appear as irregularly shaped particles with flat surfaces and sharp edges. Together with the SEM analysis also the EDX examination was performed. Most of the particle samples showed only the emission lines of the mother particles in the EDX diagram. However, some particles showed the presence of metals probably due to metallic impurities deriving from the ball milling process. Unfortunately, other details of the material cannot be provided for confidentiality reasons.

According with the results reported by Chirone et al. [33] DTA and TGA reveal a similar thermal behavior of the powder samples. The constant weight of the sample above 100 °C indicates that chemical reactions (e.g. oxidation) can be excluded in that range. The thermal behaviour observed for all the other samples was qualitatively similar.

2.3. Procedures

The minimum fluidization velocity, u_{mf}, was experimentally measured at increasing temperature. At each temperature, the u_{mf} was graphically obtained from the fluidization curves, i.e. the diagrams of the pressure drop profile across the bed over the fluidizing gas velocity, as the intersection of diagonal line and the horizontal line obtained when decreasing the gas flow rate in Fig. 3. Nitrogen was the fluidizing gas and its rate was controlled by calibrated rotameters. The fluidization curves were obtained first by increasing the gas flow rate from zero till the bed was well fluidized, and then by decreasing the flow rate to zero. Measurements were repeated, from 3 to 5 times, to increase the statistical significance of results and verify the internal consistency of the measurements. The experimental value of the pressure drops across the bed, ΔP_m, was compared with the predicted, ΔP_c ($\Delta P_c = Mg/A_c$, where M, A_c and g are the bed material weight, the cross-sectional area occupied by the material and the acceleration due to the gravity). The minimum fluidization velocity was measured from ambient temperature up to 500 °C, in steps of 100 °C. In order to guarantee a good mixing of particles the bed material was fluidized in bubble regime for around 20 min before any measurements was made.

Table 1
Characteristic sizes of the samples tested.

Sample name	A1	A2	A3	A4	A5
d_{32}, μm	7.0	22	29	65	104
d_{43},μm	14	37	63	89	227
d_{10}, μm	3.0	18	38	55	90
d_{50}, μm	12	35	61	87	184
d_{90}, μm	28	61	95	130	423
F_{45}, %	99	76.7	24.4	4.7	0
Geldart Group	C	A/C	A	A/B	B
d_{fd}, μm	–	31	43	45	96

The experimental values of u_{mf} were also compared with some of the available correlations used to predict the minimum fluidization condition. In particular, the experimental values were compared with the Baeyens and Geldart [35] Eq. (1), the viscosity term of the Wen and Yu [36] Eq. (2) and the viscous flow term of the Ergun Eq. (3):

$$u_{mf} = \frac{0.0009\left(\rho_p - \rho_g\right)^{0.934} g^{0.934} d_p^{1.8}}{\rho_g^{0.066}\mu^{0.87}} \tag{1}$$

$$u_{mf} = \frac{\left(\rho_p - \rho_g\right) g\, d_p^2}{1650\,\mu} \tag{2}$$

$$u_{mf} = \frac{\left(\rho_p - \rho_g\right) g(\varphi d_p)^2}{150\,\mu}\frac{\varepsilon_{mf}^3}{1-\varepsilon_{mf}} \tag{3}$$

It is worth noting that while the Wen and Yu [36] and the Baeyens and Geldart [35] correlations do not require a value of the bed voidage, the Ergun equation, instead, include voidage. In this latter case, estimates will be carried out using for the voidage the tapped bed value, ε_{tapped}, measured before any fluidization experiments at ambient temperature.

The bed expansion curve, i.e. the bed height as a function of the fluidizing gas rate, was obtained using the X-rays imaging technique. The bed material was initially vigorously fluidized to allow a good mixing of the particles, and then the expansion curves were obtained by slowly re-fluidizing the powder and recording the bed height at each gas velocity. Before recording the bed height, some time was allowed in order to stabilize the bed fluidization. It is also worth pointing out that the expansion profiles were obtained with several repeated experiments. The expansion curves were calculated between ambient temperature and 500 °C. At each height, the corresponding average bed voidage was also calculated with the following equation.

$$\varepsilon = 1 - \frac{M}{Ac\,\rho_p\,H} \tag{4}$$

3. Results and discussion

3.1. Experimental results: u_{mf} and ε_{mf}

Fluidization curves from ambient temperature up to 500 °C are reported in Figs. 4 and 5 for samples A5 and A4 in terms of $\Delta P_m/\Delta P_c$ ratios as a function of the gas superficial velocity. In particular, ΔP_m is the measured pressure drop and ΔP_c is the theoretical value of pressure drop at fluidization. The geometry of the symbols identifies different operating conditions. The tests were repeated from three to five times in order to increase the validity of the measurement and the values plotted are the mean values. Furthermore, the error bars were reported only in case of poor repeatability. Fig. 4a reports report the pressure drop profile obtained decreasing the gas flow rate at all temperatures. Whereas Fig. 4b reports the comparison between fluidizing and defluidizing pressure drop profiles. For gas flow rates above the minimum for fluidization, the $\Delta P_m/\Delta P_c$ ratio was constantly equal to unity in the whole range of temperatures tested. This result indicates a good fluidization quality and a negligible effect of interparticle forces in the range of temperatures of interest. According to Figs. 4 and 5, the fixed bed branch of the fluidization curve moves towards the left with the temperature, indicating higher pressure drops through the bed at equal fluid velocity. Consequently, also the minimum fluidization condition, the velocity at which the bed is fully supported by the gas, occurs at lower velocity

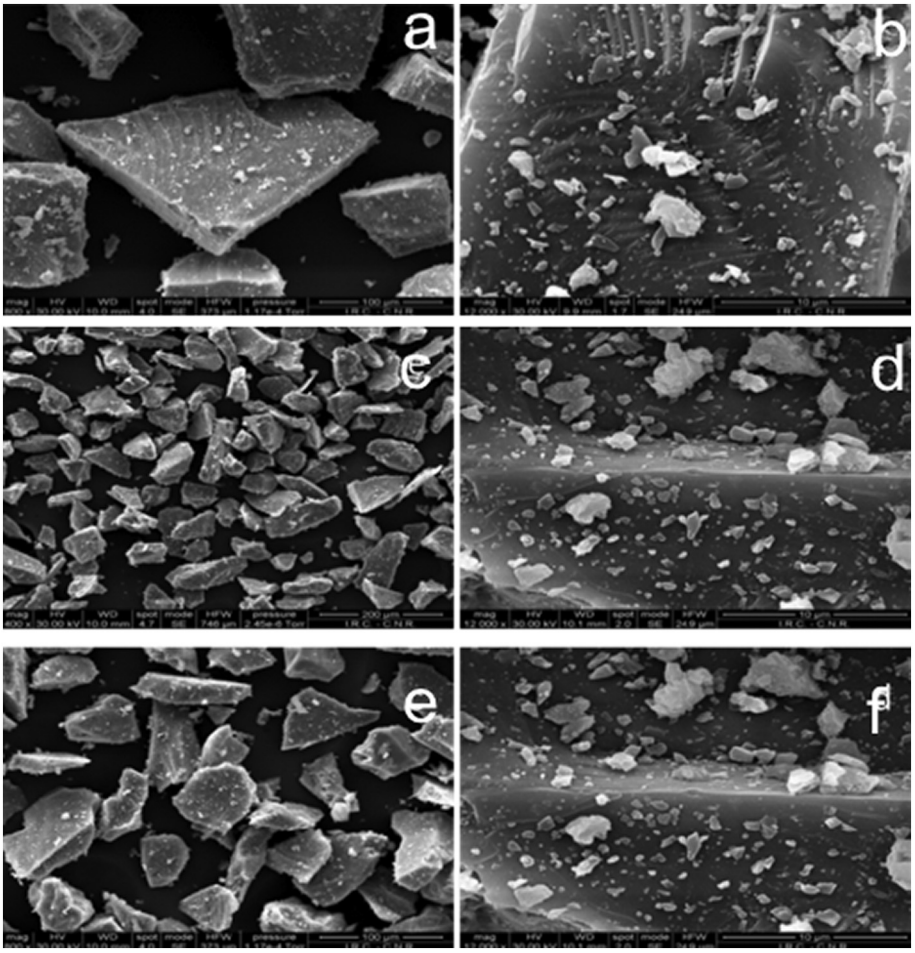

Fig. 2. SEM pictures sample A5 (a, b), A3 (c, d) and A1 (e, f).

and therefore, the experimental value u_{mf} decreases with increasing temperature for both samples.

Fluidization curves of samples A3 and A2 are reported in Figs. 6 and 7. Similarly, with these samples, for flow rates well above the minimum fluidization condition, the ΔP_m value equals the theoretical fluidization value ΔP_c at all the tested temperatures. In this case, the fluidization curves shift towards the left only up to temperatures of 400 °C and 300 °C for the sample A3 and A2 respectively. In fact, for sample A3 an increase of temperature above 400 has a limited effect on the fluidization curves (Fig. 6b) that remains almost constant, and thus on the minimum fluidization condition, such as the u_{mf} value. Whereas for Sample A2, a further increase of temperature beyond 400 °C, caused an inversion of the curve shift with temperature and an increase of u_{mf} is observed (Fig. 7b). It should also be noted that when increasing the temperature, the reproducibility of the experimental measurements became much lower, as it appears from the larger error bars.

While increasing the gas flow rate, four different stages can be identified for both samples A3 and A2:

- Stage 1: At low gas velocity, ΔP increases almost linearly with the flow rate.
- Stage 2: Further increasing the gas velocity, the ratio $\Delta P_m/\Delta P_c$ reaches its maximum value, larger than 1.
- Stage 3: At just larger gas velocities, small bubbles are seen breaking the surface and travelling through the bed in instable channelling. In the whole range of temperatures tested, the raito $\Delta P_m/\Delta P_c$ remains below 70–80% for sample A3 and below 70–50% for sample A2. Further increasing the gas flow rate, the pressure drop ΔP_m approaches ΔP_c as a consequence of the disruption of the formed channels (Fig. 8).
- Stage 4: At the highest gas velocities tested, larger bubbles are seen all over the surface and the ratio $\Delta P_m/\Delta P_c = 1$

During stage 3, the fluidization behaviour was mainly characterized by unstable channelling fluidization, resulting in highly variable values of the ratio $\Delta P_m/\Delta P_c$, as shown in Fig. 8. To better explain the fluidization behaviour, Fig. 9 reports an X-ray image of the inside of the reactor for sample A2. Images are taken at four different gas velocities, 0.12, 0.3, 0.4 and 0.8 cm/s. Inspection of the images suggests that the unstable

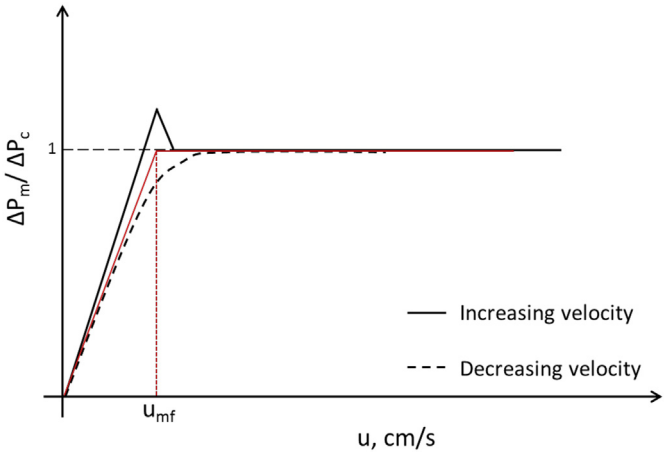

Fig. 3. Typical fluidization curves for powders belonging to the Group A of the Geldart [3] classification.

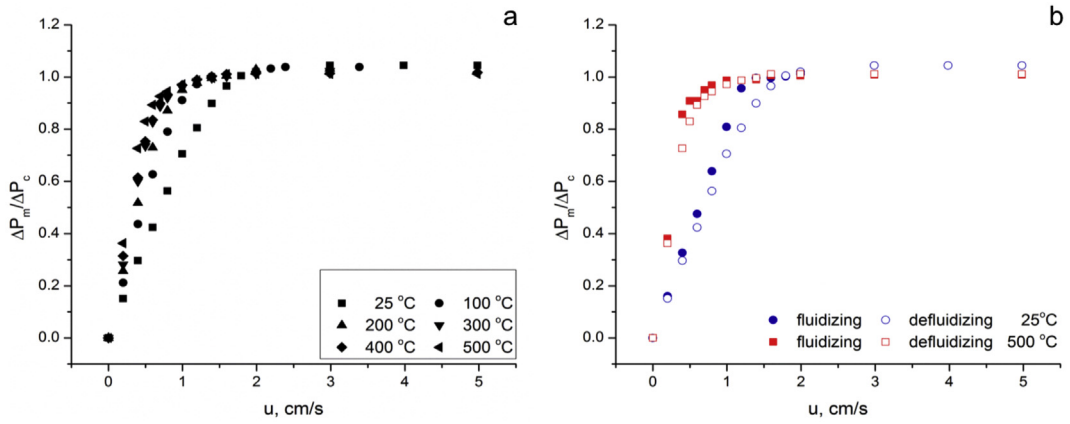

Fig. 4. Pressure drop as a function of fluidization velocity for Sample A5: a) defluidization experiments at changing temperature; b) fluidization and defluidization experiments at changing temperatures. Pressure drops are expressed in terms of the ratio of the measured values and the theoretical for fluidization.

pressure drop profile between 0.15 and 0.6 cm/s is due to irregular bypass of the gas through the bed particles causing vertical channels. At $u < u_{mf}$, Fig. 9a shows a fixed bed. Increasing the gas flow rate, the pressure drop starts to fluctuate and, according with Fig. 9b, a non-horizontal bed surface can be observed. In video sequences, corresponding to the depression of the bed surface, it is possible to observe local variations of bed density, visible as fluctuations of the image grey levels, and of the bed surface, that can clearly be attributed to high gas velocity in the region due to channelling. A further increase of the flow rate causes an expansion of the channel, a lower bed surface still non-horizontal (visible from the video sequences in the supplement material), with a consequent linear increase of the pressure drop (Fig. 9c).

For particular operating temperature and powder samples, it is also noticeable a pressure drop peak in the fluidization curve at increasing gas velocity close to the minimum for fluidization, corresponding to values of the ratio $\Delta P_m/\Delta P_c$ significantly larger than 1. This overshoot can be an indication of some degree of cohesiveness of the bed particles. The values of the overshoot are reported in Fig. 10 for both samples. The Figure shows an increase of the ratio $\Delta P_m/\Delta P_c$ up to 300 °C. Instead between 300 and 500 °C the ratio is almost constant.

Moreover, hysteresis phenomena were observed during fluidization and defluidization cycles. Hysteresis phenomena are more evident for sample A2, the most cohesive powder among those discussed above, at high temperatures (Fig. 8).

The finest sample tested, A1, belongs to the Group C of the Geldart classification. This powder sample is characterized by a very high degree of cohesiveness. In fact, fluidization conditions could not be achieved at any temperatures between ambient and 500 °C, due to the dominant role of interparticle forces over hydrodynamic forces. Figs. 11 and 12 report the fluidization curves at ambient condition and the snapshots of the reactor at superficial gas velocities of 0, 0.9, 1.0, 2.2, 5.0 and 6.5 cm/s, respectively. From the X-rays images the structure of the bed can be observed. Inspection of Fig. 12 indicates that channelling phenomena occur and, particularly at the higher flow rates, it becomes clear that the channels develop as horizontal cracks, such as those that, in similar cases, might lead to the phenomenon of solid plugs rising and breaking.

The bed voidage at the minimum velocity for fluidization, ε_{mf}, was estimated from the bed height measured with the X-ray images of the bed. In particular, the bed voidage was calculated using Eq. (4) and it is reported in Fig. 13. All the samples show a steady increase of the bed voidage with temperature. A maximum value of the relative voidage increase was observed for the finest sample A2 that was calculated to be 15% and around 7% for the other samples. The Ergun correlation (Eq. (3)) was also used to calculate the particle sphericity, φ, of each samples using the experimental values of u_{mf} and ε_{mf} at ambient temperature as suggested by Knowlton [20]. Unfortunately, the procedure led to unrealistic values of the sphericity between 1 and 1.2 that could not be used. Consequently, the shape factor of the particles was geometrically estimated using the SEM pictures and considering a parallelepiped shape of the particles. In particular, the prevalent dimension of the parallelepiped was considered. The results show values of φ between 0.68 and 0.75. Thus, a constant value of $\varphi = 0.7$ was considered

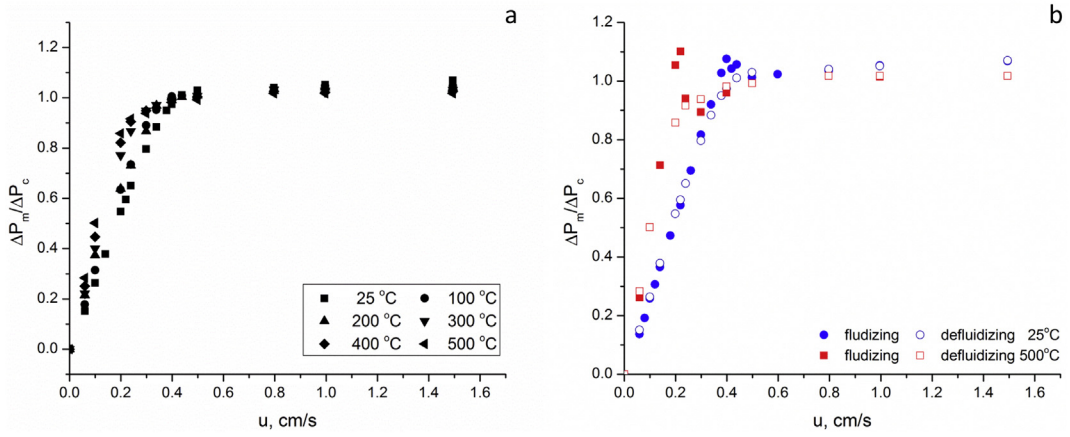

Fig. 5. Pressure drop as a function of fluidization velocity for Sample A4: a) defluidization experiments at changing temperature; b) fluidization and defluidization experiments at changing temperatures. Pressure drops are expressed in terms of the ratio of the measured values and the theoretical for fluidization.

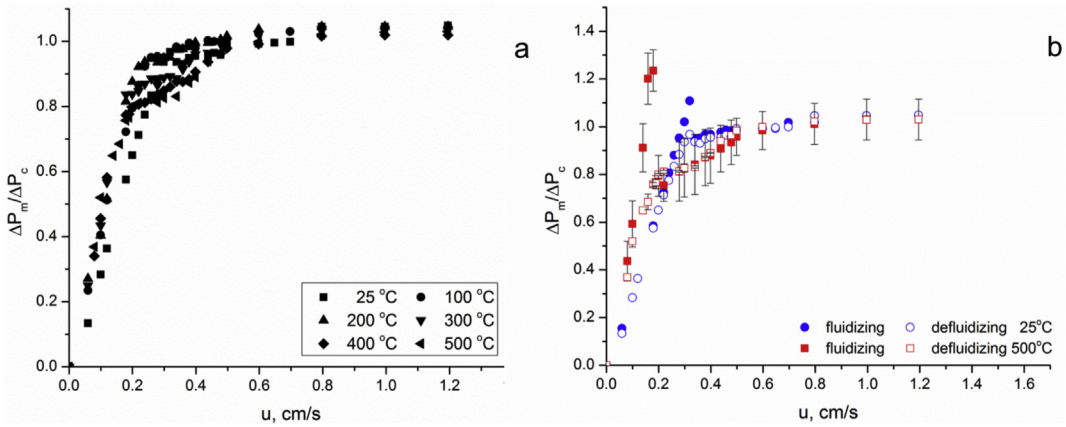

Fig. 6. Pressure drop as a function of fluidization velocity for Sample A3: a) defluidization experiments at changing temperature; b) fluidization and defluidization experiments at changing temperatures. Pressure drops are expressed in terms of the ratio of the measured values and the theoretical for fluidization.

and this value was used to estimate an effective fluid dynamic particle diameter d_{fd} also reported in Table 1.

3.1.1. Relationship between the pressure overshoot and the powder flow properties

In cohesive powder systems, the tensile strength represents a fundamental mechanical property of a powder in handling issues [37,38]. Generally, it can be determinate indirectly from the yield locus by linear or curve extrapolation [33,39,40]. On the other hand, it can directly be measured with split cell tester [41–43] or lifting lid tester [44]. The main issue of these apparatus is the non-uniform stress distribution inside the powder sample that cause a poor reproducibility of the results in case of fine cohesive powders.

A fluidized bed system with a certain degree of particle cohesiveness generally shows some pressure overshoot during the fluidization branch of the pressure drop profile. The direct connection between the pressure overshot and the powder flow properties is still a debated question. According to Castellanos et al. [45] the pressure overshoot, that is the difference between the peak pressure and the theoretical fluidization pressure drop equals the tensile strength of the material that can withstand the overpressure only for values lower than those corresponding to the material break at the pressure peak.

$$\frac{\Delta P_{overshoot}}{\Delta P_c} = \frac{\sigma_t}{\rho(1-\varepsilon)gH} + 1 \tag{5}$$

Where σ_t is the tensile strength at the base of the bed. Following this approach, it was possible to use the estimation of the tensile strength based on the measurement of powder flow properties made at ambient and high temperature and reported in a previous paper [33], in order to verify if the change of interparticle forces with temperature can explain the changes observed in the overpressure.

The bed weight determines the powder consolidation at the bottom and therefore:

$$\sigma_1 = \rho(1-\varepsilon)gH \tag{6}$$

Zafar et al. [46] report experimental measurement results of the tensile strength of different powder samples determined by both direct, such as Sevilla Powder Tester and Raining Bed Method, and indirect techniques, extrapolated from the results of the Schulze Shear Cell. They found qualitatively similar results for the tested powders using different methods, concluding that it is fundamental to analyse in detail the conditions of powder flow for each application in order to choose the most appropriate test.

A simple model used to correlate the bulk material strength and the particle-particle properties was proposed by Rumpf [47] and Molerus [48] according to whom the following equation can be used to relate interparticle force with stresses and strength:

$$\sigma_t = \frac{F_{vdW}}{d_{sv}^2}\frac{1-\varepsilon}{\varepsilon} \tag{7}$$

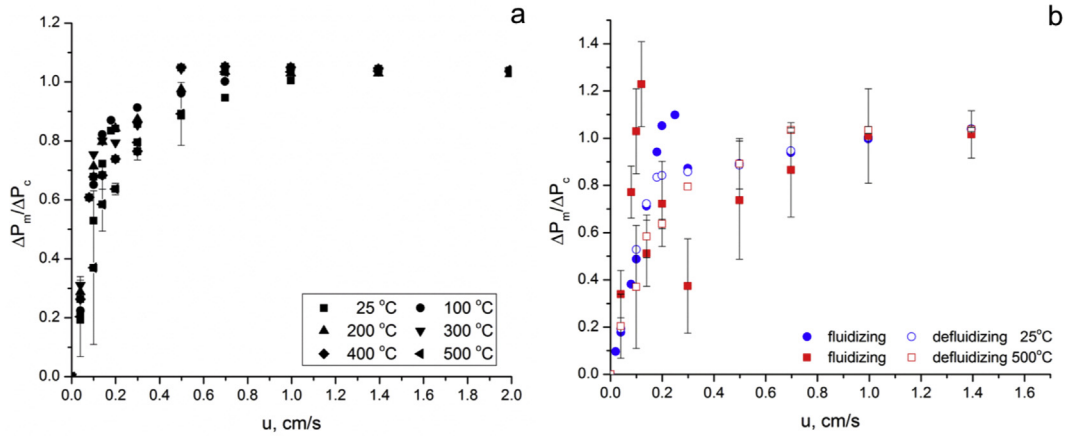

Fig. 7. Pressure drop as a function of fluidization velocity for Sample A2: a) defluidization experiments at changing temperature; b) fluidization and defluidization experiments at changing temperatures. Pressure drops are expressed in terms of the ratio of the measured values and the theoretical for fluidization.

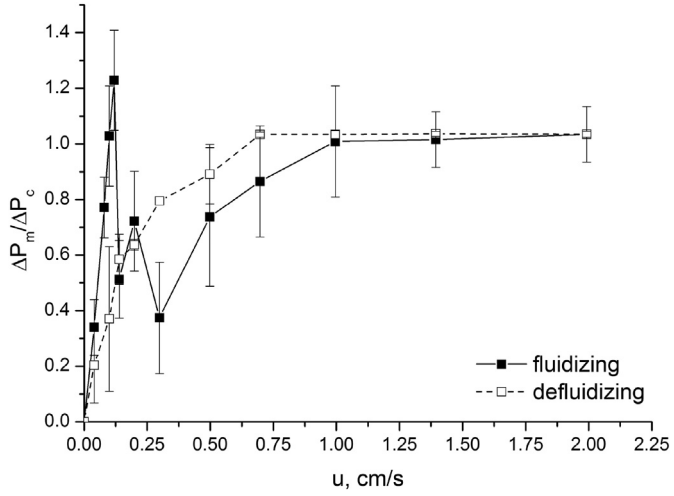

Fig. 8. Pressure drop as a function of fluidization velocity for Sample A2 for fluidizaiton and defluidization experiments at at 500 °C. Pressure drops are expressed in terms of the ratio of the measured values and the theoretical for fluidization.

$$\sigma_1 = \frac{F_N}{{d_{sv}}^2}\frac{1-\varepsilon}{\varepsilon} \tag{8}$$

The applicability of the model, especially for very low consolidated systems of particles, can be still considered debatable. However, in the past, the combined use of the tensile strength extrapolated from the yield locus and of Eq. (7) was successfully used for several applications.

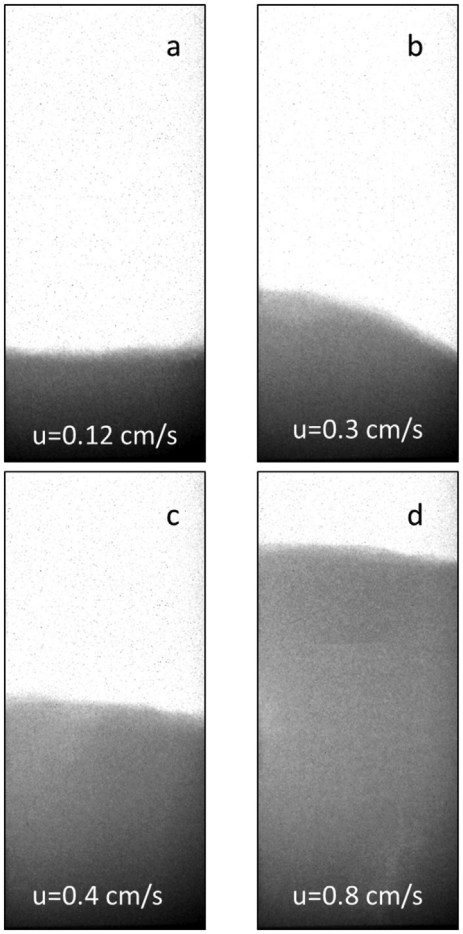

Fig. 9. X-rays images of the reactor for sample A2 at different flow rate at 500 °C.

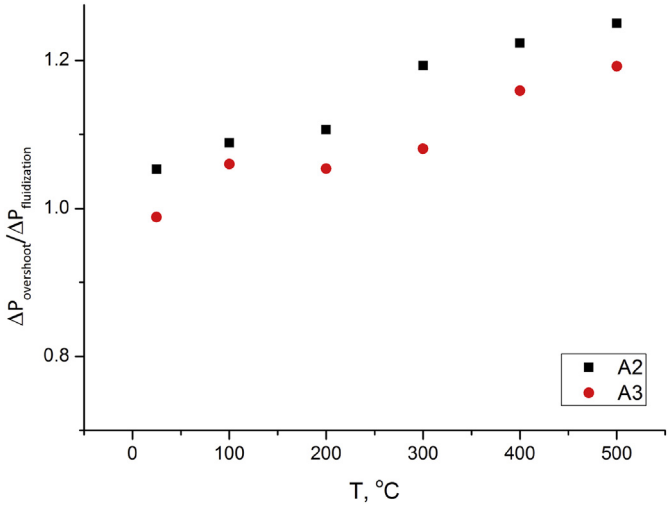

Fig. 10. Effect of temperature on the overshoot, expressed with the ratio $\Delta P_{overshoot}/\Delta P_{fluidization}$, for sample A3 and A2.

Tomasetta et al. [49] found that Molerus equation (Eq. (7)) with the assumption of plastic deformation provides the correct order of magnitude values of tensile strength extrapolated from the powder yield locus and, more significantly, its dependence on consolidation. Furthermore, more accurate studies carried on ceramic powders demonstrated that, by using a reasonable value of the mean curvature radius at the contact points, the tensile strength and its dependence with the particle diameter, the applied consolidation and the system temperature are correctly predicted with the with the use of Eqs. (7) and (8), together with the tensile strength extrapolated from a yield locus [33]. A direct confirmation of the appropriateness of the procedure was found by comparing the interparticle forces calculated by Chirone et al. [33] with the interparticle forces calculated from experiments of sound assisted fluidization on the same powders [50]. In particular, the results confirmed the applicability of both methodologies for the estimation of the interpaticle forces under different consolidation state.

$$F_{vdW} = \frac{\mathrm{Ar}}{12{z_0}^2}\frac{1+\dfrac{2F_N}{\pi p_f r z_0}}{1-\dfrac{A}{6\pi p_f {z_0}^3}} \tag{9}$$

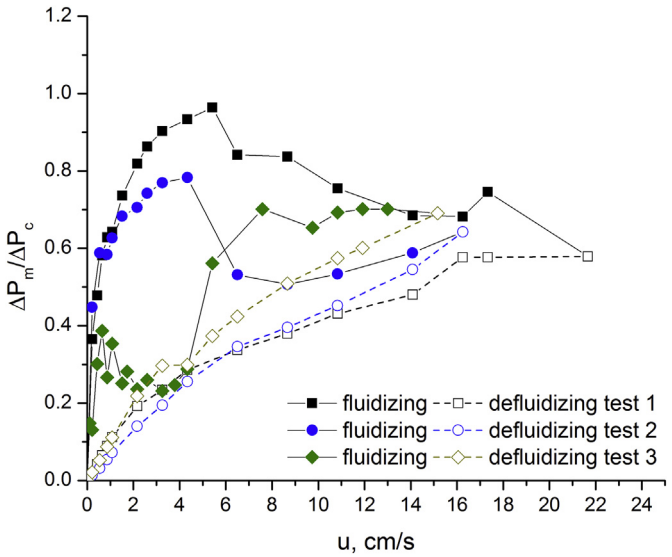

Fig. 11. Pressure drop versus gas fluidization velocity for sample A1 at ambient condition.

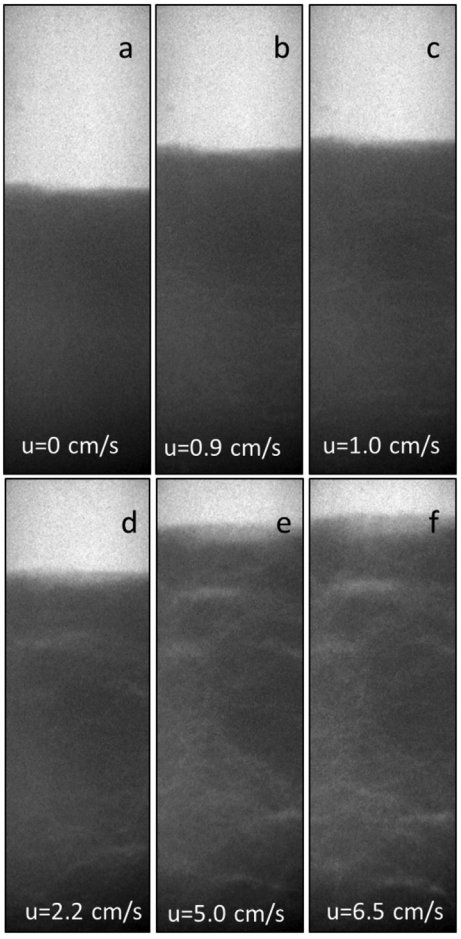

Fig. 12. Snapshot inside the reactor of sample A1 at ambient condition at different gas flow rates.

It was also found that in presence of a liquid phase, after a reasonable estimation of the capillary interparticle forces, Eq. (7) is able to correctly predict the order of magnitude of the tensile strength extrapolated from the powder yield loci, as well as, its variations with temperature [51]. Other successful applications of the same approach used to relate the tensile strength of yield loci and interparticle forces with Eq. (7) as a function of consolidation forces estimated with Eq. (8) are reported by

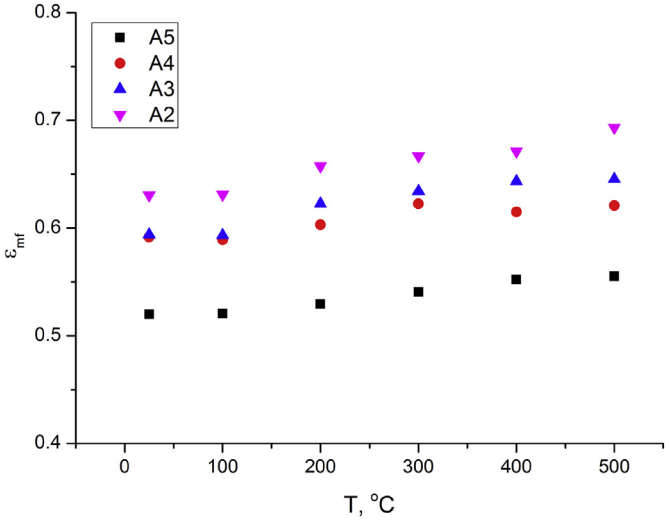

Fig. 13. Effect of temperature on the bed voidage at the minimum gas velocity for fluidization.

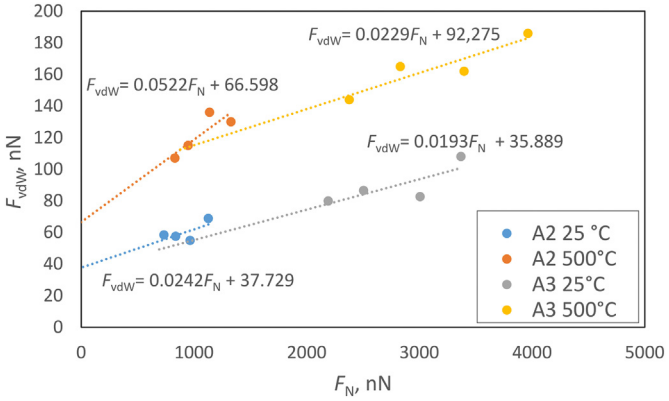

Fig. 14. Tensile Strength as function of the consolidation forces from in [34].

Macrì et al. [52,53] with reference to the flow properties of Titania powders at different temperatures, by Liu et al. [54] for ashes at different temperature and by Liu et al. [55]for coal. In this latter case a modified version of Eq. (7) was developed to account for wide particle size distribution of the particulate systems. Eq. (7) and this latter modification were successfully used to relate the strength of interparticle connection with the material tensile strength in selective laser sintered artefact obtained by unimodal [56] and bimodal [57] powder samples, respectively. Independent proofs of the significance of the tensile strength of powder obtained from extrapolation from yield loci are provided by Barletta et al. [58] and by Barletta and Poletto [59] who were able, with that, to correctly predict the aggregates size of cohesive powders in the aerated discharge from hoppers and in gas fluidization assisted by mechanical vibrations, respectively.

Provided the above and, therefore, assuming that Eqs. (5) to (8) as well as the extrapolation of the tensile strength from the yield locus and the pressure overshoot gas fluidization can be assumed valid with a reasonable degree of confidence, a linear relationship is adequate to relate F_{vdW} and F_N

$$F_{vdW} = a + b\,F_N \tag{10}$$

In [33] data of F_{vdW} and F_N estimated with Eqs. (7) and (8) from linear extrapolation of the tensile strength from powder yield loci and the corresponding values of σ_1 were available for powders A2 and A3 at ambient temperature and at 500 °C. These are reported in Fig. 14 together with linear correlation function of the kind of Eq. (10).

Considering the same powders at the same temperature inside the fluidized bed, Table 2 reports the values of $\sigma_1$calculated according to Eq. (6), F_N values calculated according to Eq. (9). Furthermore F_{vdW} were calculated assuming that regression Eq. (10) with the coefficient values reported in Fig. 14 apply in our fluidized bed. Finally, on these bases σ_t values were calculated using Eq. (8) and values of the ratios $\Delta P_{overshoot}/\Delta P_c$ applying Eq. (5).

The comparison of the calculated values of the pressure overshoots and the experimental ones is reported in Fig. 15.

The results show that the experimental overshoots at high temperature are much larger than those estimated from powder flow properties. Since the procedure adopted to estimate σ_t from powder flow

Table 2
Sample parameters for the mathematical estimation of the ratios $\Delta P_{overshoot}/\Delta P_c$.

Powder	T	H	ε	σ_1	F_N	F_{vdW}	σ_t	$\Delta P_{overshoot}/\Delta P_c$
–	°C	mm	–	Pa	nN	nN	Pa	–
A2	25	245	0.56	2464	1588	76	103	1.05
A2	500	273	0.62	2371	1959	169	166	1.09
A3	25	369	0.49	4302	6779	167	128	1.02
A3	500	390	0.53	4190	7750	270	255	1.03

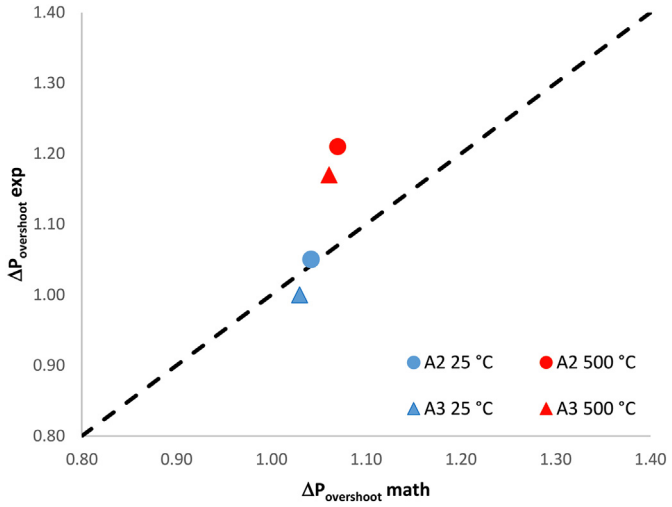

Fig. 15. Mathematical pressure overshoot vs experimental pressure overshoot for sample A3 and A2.

properties uses a linear extrapolation of the yield locus on the traction side, it is known that it tends to somewhat overestimates values of the tensile strength [42]. The fact that, in spite of this theoretical overestimation, fluidization results provide larger overpressure suggests that the pressure overshoots in these experiments cannot be explained only by considering an increase of interparticle forces affecting the bed cohesion. Instead it is possible that other indirect effects of interparticle forces such as the bed adhesion on the column walls may play a significant role. This is likely in a fluidized bed system with a high ratio between the height and the diameter (in our experiments this ratio is around 2).

3.2. Experimental result: bed expansion curves

The bed expansion curves were determined from the X-ray imaging technique and following the experimental procedure described in the previous section. The expansion curves reported in the following are the result of an averaging procedure over several (3–4) repeated experiments. The bed expansion curves obtained for all the samples at each temperature are reported in Fig. 16 and they show similar characteristics for all the samples tested. A maximum bed expansion value is obtained at temperatures around 300/400 °C. The results of the thermogravimetric analysis showed no weight loss in the temperature range of interest for all powder samples, thus this maximum cannot be justified with changes of the sample weight. Instead these temperature effects on the bed expansion it can be explained by the combined effects of temperature on both the gas properties and the particle compressive strength p_f [60]. In particular, for temperatures between 25 °C and 300 °C, it is likely that the temperature mainly affects the gas properties (density and viscosity), instead, for temperatures higher than 300 °C, the particles show a significant decrease of the compressive strength [60] with a relative increase of the interparticle forces. The gas velocity, at which the bed expansion starts, decreases with temperature, while the magnitude of the expansion increases with temperature and with decreasing average particle size of the sample, as shown in Fig. 17.

A considerable increase of the bed expansion occurred for all the samples from 20 °C up to 300 °C: a 15% relative increase was observed for the A5 and A4 sample, about 24% for A3, and a relative increase of up to 50% was observed for A2.

Fig. 18 shows the comparison of the bed height recorded while increasing and while decreasing the gas flow rate. Slight hysteresis phenomena can be observed at high temperature for samples A3 and A2.

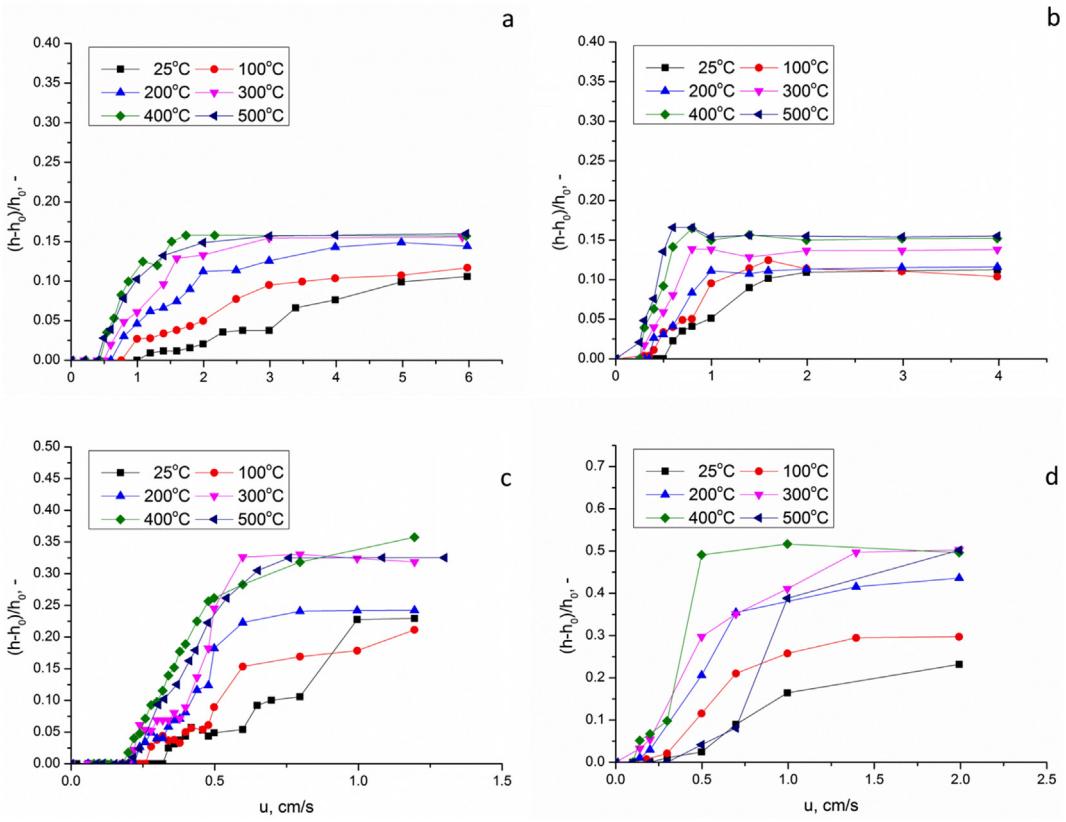

Fig. 16. Effect of temperature on bed expansion curves of the different samples: a) A5; b) A4; c) A3; d) A2.

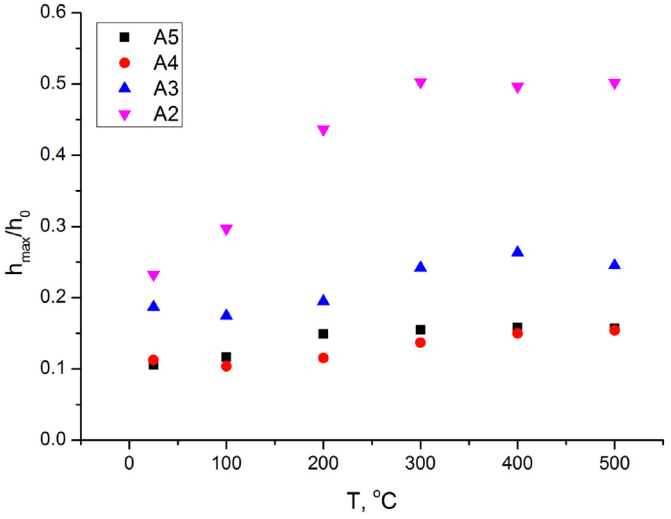

Fig. 17. Effect of temperature on the ratio h_{max}/h_0 for all the materials.

3.2.1. The settled voidage of the bed

Fig. 19 reports the settled bed voidage calculated in slow and fast defluidization experiments as a function of temperature for all the tested powders. In both cases of slow and fast defluidization the starting conditions was a well-established bubbling condition. The slow defluidization experiment was achieved with small decremental steps of the gas flow rate. Whereas, the fast defluidization was obtained with a sudden cut off of the gas supply.

The settled bed voidage, ε_s, was found to increase with temperature of about 9% in both cases of slow and fast defluidization experiments. The same trend with temperature was also found by Lettieri in experiments carried out on FCC powders [21]. The ε_s values obtained from fast defluidization experiments were found to be a little larger for all the materials than those measured in slow defluidization experiments.

3.2.2. The bed expansion profile in Richardson-Zaki form

The bed expansion in the range of homogenous fluidization was also investigated by using the Richardson-Zaki equation, Eq. (11) [61].

$$u = u_t \varepsilon^n \tag{11}$$

where u_t represents the terminal velocity of a single particle and n is an index that, according to Richardson and Zaki [61], should depend on the system fluid dynamics. The values of u_t and n that were obtained by fitting Eq. (11) on the expansion curves are denoted as n^* and u_t^* and will be addressed to as experimental values. The fitting procedure was carried out by plotting the fluidizing velocity and the voidage, on logarithmic scales, on which Eq. (11) should appear as a line and a linear regression procedure on data can be adopted. Fig. 20 shows the results of this fitting procedure on all the expansion curve.

For samples A5 and A4 a single slope line could be used to fit data in the whole expansion range of the bed, as shown in Fig. 20a–b. The expansion profiles of samples A3 and A4 are better described by using two different lines to fit the data at low and large values of the bed expansion (the fitting equations are reported in Table 3). The values of the voidage, $\varepsilon_{changing\ slope}$, which identify the slope changes, are reported in Fig. 21 and Table 3. An increase of $\varepsilon_{changing\ slope}$ with temperature was observed. It can be argued that this parameter can identify the point at which the interparticle forces and hydrodynamic forces change they relative significance. At values of $\varepsilon < \varepsilon_{changing\ slope}$ the slope of the expansion curve is higher than at values of $\varepsilon > \varepsilon_{changing\ slope}$. Larger slopes in the lines of Fig. 21 mean larger values of the exponent *n* of the Richardson and Zaki equation. These may suggest the presence of other forces affecting the bed expansion than purely fluid dynamic interaction. Interparticle forces may induce the formation of internal structures in the bed that support part of the bed weight, keep the bed expanded

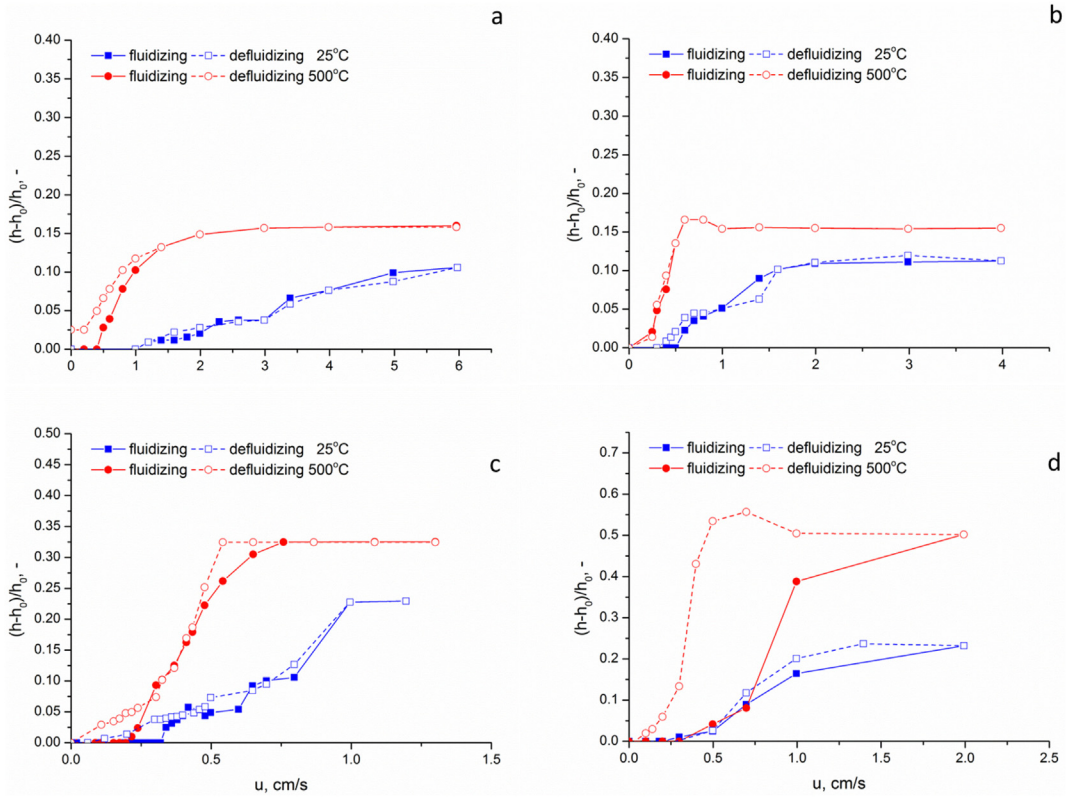

Fig. 18. Comparison fluidizing and defluidizing profile for sample a) samples A5; b) sample A4. c) sample A3; d) sample A2.

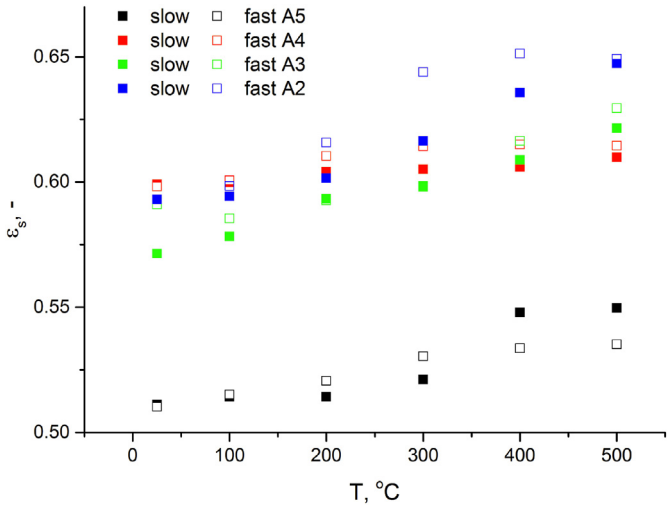

Fig. 19. Effect of temperature of the settling procedure on the settled voidage of the bed. Slow settling procedure is obtained while slightly decreasing the flow rate and fast settling procedure is obtained when suddenly cutting off the gas supply.

and, therefore, reduce the ability of the fluid velocity change to produce a significant change of the bed expansion, if referred to the case in which expansion is purely driven by only fluid dynamic forces. These structures are stable only at the lowest bed voidages and, perhaps, for $\varepsilon < \varepsilon_{changing\ slope}$. At higher bed expansion, for $\varepsilon < \varepsilon_{changing\ slope}$, the particles tend to be fluidized as separate particles and, therefore, the variation of bed height with fluidization velocity is less pronounced. It is consistent with this interpretation the fact that at higher temperatures, when interparticle forces become more important change in the slope are more significant.

Figs. 22 and 23 show the effect of temperature on the index n* (slope of the line regression on Fig. 20 for $\varepsilon < \varepsilon_{changing\ slope}$) and the values of u_t^* (the line intercept at $\varepsilon = 1$). Both parameters decrease in the range of temperatures investigated. These results are in agreement with those reported by Lettieri et al [21] These experimental values were also compared with the predicted values of n and u_t obtained according to Richardson and Zaki [61]. In this case the values of u_t can be obtained from the theory of terminal velocity, the values of n from the empirical equations derived by Richardson and Zaki [61] for homogeneous fluidization governed by purely fluid dynamic interactions. The following relations were used to estimate the terminal velocity u_t and the index n:

$$\begin{array}{ll} Ga = 18\ Re_t & \text{for}\quad Ga \le 3.6 \\ Ga = 18\ Re_t + 2.7\ Re_t^{1.687} & \text{for}\quad 3.6 \le Ga \le 500 \end{array} \tag{12}$$

$$\begin{array}{ll} n = 4.8 & Re_t \le 0.2 \\ n = 4.6\ Re_t^{-0.03} & 0.2 \le Re_t \le 1 \\ n = 4.6\ Re_t^{-0.1} & 1 \le Re_t \le 500 \end{array} \tag{13}$$

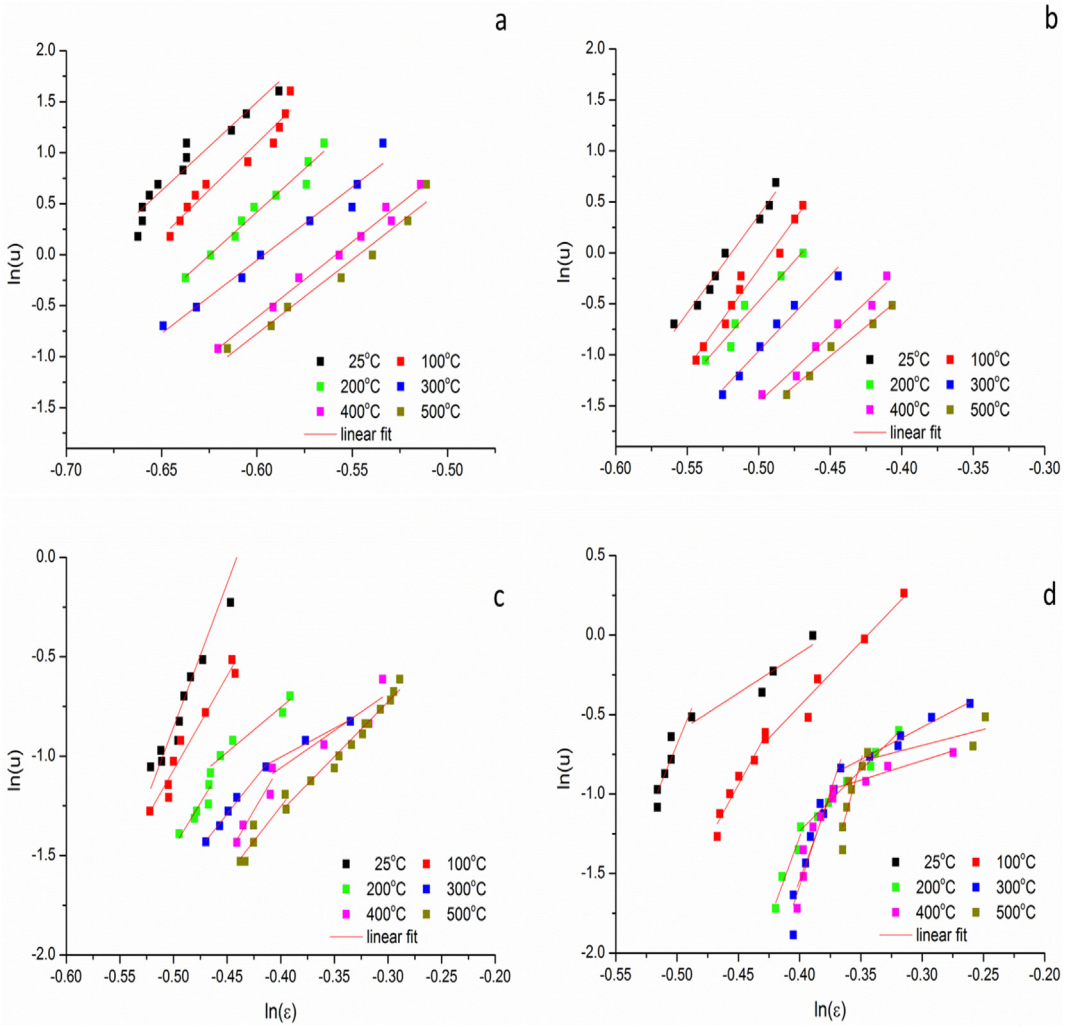

Fig. 20. Bed expansion in the Richardson-Zaki form profile for sample a) samples A5; b) sample A4. c) sample A3; d) sample A2.

Table 3
Linear regression fitting the data at low and large values of the bed expansion for sample A2 and A3.

T, °C	$\varepsilon < \varepsilon_{changing\ slope}$			$\varepsilon > \varepsilon_{changing\ slope}$			$\varepsilon_{changing\ slope}$	$u_{changing\ slope}$, cm/s
	n	u_t	R^2	n	u_t	R^2		
Sample A2								
25	16.29	7.47	0.87	5.01	1.89	0.91	0.61	0.60
100	14.18	5.44	0.96	8.04	2.77	0.96	0.65	0.54
200	16.40	5.24	0.90	7.96	1.94	0.99	0.67	0.31
300	28.52	9.82	0.90	4.96	0.91	0.95	0.67	0.35
400	28.49	9.83	0.88	2.44	0.06	0.95	0.67	0.38
500	32.66	10.71	0.99	1.99	0.09	0.68	0.70	0.48
Sample A3								
25	12.13	5.21	0.99				–	–
100	9.49	3.67	0.96				–	–
200	10.16	3. 58	0.87	4.07	0.87	0.96	0.63	0.37
300	6.82	1.78	0.99	2.89	0.15	0.98	0.67	0.35
400	9.24	2.65	0.91	3.75	0.44	0.84	0.67	0.34
500	6.93	1.52	0.87	5.52	0.93	0.97	0.67	0.30

where Re_t is the dimensionless Reynolds number referred to the terminal particle velocity and *Ga* is the dimensionless Galileo number.

Table 4 reports the values of n and u_t predicted according to Eqs. 12 and 13 and the corresponding experimental values obtained with the fitting procedure shown in Fig. 20 for all sample tested and temperatures and for $\varepsilon < \varepsilon_{changing\ slope}$. Due to the small particle size that constrain the fluid particle system to the viscous regime, the predicted values for n are all 4.8. As expected for the viscous regime in which the effect on the terminal velocity is determined by the increase of the gas viscosity, the calculated values of u_t decrease with temperature. Similar trends are observed for the experiment al values u_t^*, with the exception for the finest sample A2. Despite the similar trends, the calculated values of u_t are greater than the experimental values of u_t^* for samples A5 and A4, they are similar for sample A3, while they are smaller for the sample A2.

4. Discussions

The experimental results show that the mean particle size affects significantly the fluidization behaviour of the materials investigated. In particular, significant differences were observed in the fluidization behaviour of the coarsest samples A5, A4 and the finest sample A3, A2. The sample A1, which exhibits the highest cohesion, was impossible to fluidize with an ordinary fluidized bed reactor. For all materials tested, the ratio $\Delta P_m/\Delta P_c$ provided the very first indication on the influence of the HDFs and IPFs on the fluidization behaviour. The measured pressure drops across the bed, ΔP_m, was within 1 or 2% of the theoretical value ΔP_c for all fresh material tested, indicating that the bed material was relatively free from any dominant effect of the interparticle forces. However, an increase in the pressure deviation of the pressure drops with increasing temperature was observed to occur when the role of the IPFs was enhanced due to the increase of temperature. Hysteresis phenomena were observed in the pressure drop curves for the finest samples (A3 and A2) and for temperatures higher than 400 °C. Several researches found this phenomenon associated with fluidization of nanoparticles [62,63]. A theoretical explanation for this phenomenon is based on the role of contact or yield stresses and wall friction, which results in plugging of the nanoparticle agglomerates at low velocities [63,64].

Different structures within the bed were found, as detected in the X-ray images. Vertical channels were seen to form into the bed of samples A3 and A2. Whereas, horizontal cracks were seen to form continuously within the bed of sample A1, causing the pressure drop to decrease and vary with time. This material sample was impossible to fluidize in ordinary conditions.

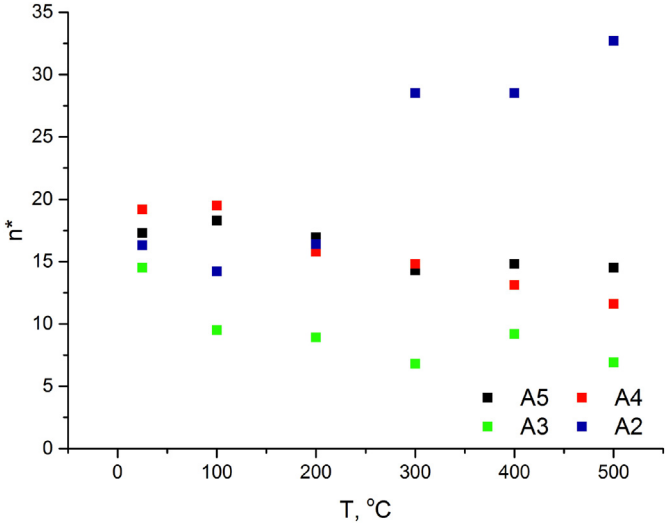

Fig. 22. Effect of temperature on the index n* of the Richardson-Zaki equation.

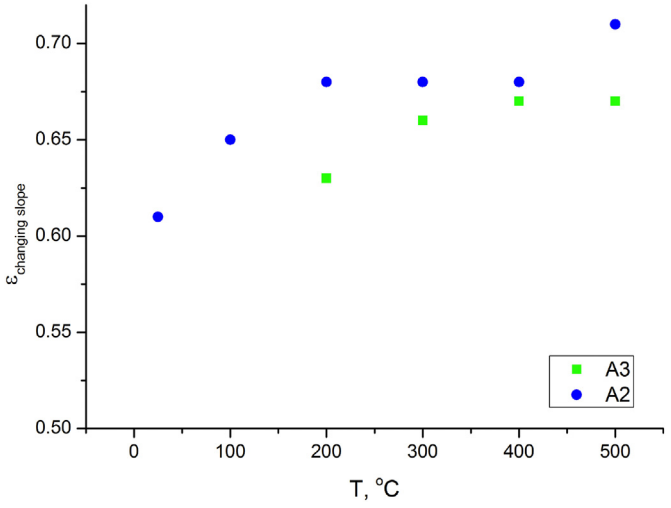

Fig. 21. Effect of temperature on the voidage at which the slope changes for the R-Z equation.

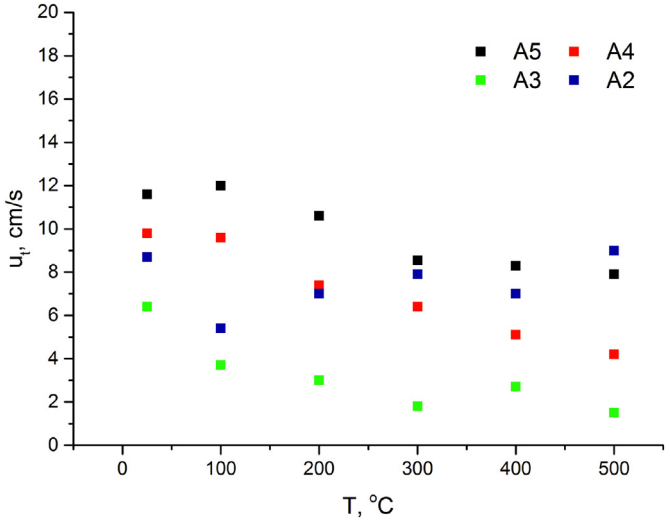

Fig. 23. Effect of temperature on u_t of the Richardson-Zaki equation.

Table 4
Comparison of the mathematical and experimental values for n and u_t of the R-Z equation.

T, °C	u_t^*	u_t	n^*	n	u_t^*	u_t	n^*	n
	A5				A4			
25	11.6	75.0	17.3	4.1	9.8	27.0	19.2	4.8
100	12.0	63.5	18.3	4.4	9.6	22.9	19.5	4.8
200	10.6	53.3	17.0	4.6	7.4	19.2	15.8	4.8
300	8.6	46.2	14.3	4.7	6.4	16.6	14.8	4.8
400	8.3	41.0	14.8	4.7	5.1	14.8	13.1	4.8
500	7.9	37.0	14.5	4.8	4.2	13.3	11.6	4.8
	A3				A2			
25	6.4	5.8	14.5	4.8	7.5	3.5	16.3	4.8
100	3.7	4.8	9.5	4.8	5.4	3.0	14.2	4.8
200	3.0	4.1	8.9	4.8	5.2	2.5	16.4	4.8
300	1.8	3.6	6.8	4.8	9.8	2.2	28.5	4.8
400	2.7	3.2	9.2	4.8	9.8	1.9	28.5	4.8
500	1.5	2.5	6.9	4.8	10.7	1.7	32.7	4.8

Regarding the effect of temperature on the minimum fluidization velocity, three different trends were found. Samples A5 and A4 show a decreasing experimental value of u_{mf} with increasing temperature. Sample A3 shows a weaker dependence of u_{mf} with temperature. Differently, u_{mf} values obtained for sample A2 decreased from 20 °C up to 200 °C as the fluidization behaviour is controlled by the HDFs, u_{mf} then suddenly increased between 300 and 500 °C when the IPFs started to become more dominant and to determine larger bed voidages. The experimental minimum fluidization velocity was compared with the Ergun equation (Eq. (3)), considering the measured bed voidage from the X-ray observation at the minimum for fluidization at each temperature. In all the cases, the value of d_{fd} was used. The calculated values of u_{mf} are reported as a black solid line in Fig. 24, where they can be compared with the experimental values reported as black dots. In the same plot also, the values of u_{mf} calculated from literature Eqs. (1) to (3) are reported. As expected, since d_{fd} is obtained by fitting the Ergun equation on experimental data at ambient temperature, it can be seen that the Ergun equation, with the experimental values of voidage at the process conditions and d_{fd} values, do provide the best agreement between calculated values and experimental values of the u_{mf}. A sensitivity analysis on the effect of the value used for ε_s in the prediction of the minimum fluidization velocity can be carried out using the predetermined values of $\varepsilon_{s,tapped}$ if in place of the experimental values determined on the basis of the bed height visualized with the X-ray set up. Fig. 24 shows that for samples A5 and A4, the Baeyens and Geldart equation, the Wen and Yu equation and the Ergun equation with the predetermined $\varepsilon_{s,tapped}$ well describe the effect of temperature on the minimum fluidization condition but underestimate the experimental values (black dotted lines). According to Table 5, the relative errors referred to the two materials for the different predictive equations not using experimental values for ε_{mf} range between 24 and 78%. Whereas, for samples A3 and A2 the comparison indicates that all the predictions not using the experimental value of ε_{mf} at the process conditions underestimate the experiments and are not even able to follow the trend of the experimental values of u_{mf} at the highest temperatures. According to Table 5, the relative errors referred to the two materials for the different predictive equations not using experimental values for ε_{mf} vary from 50% to 66% for sample A3 and from 50% to 89% for sample A2. In all the cases the relative errors of the Ergun equation with the experimentally determined value of ε_{mf} are within 15%. This finding suggests that for powders made of coarser particle the prevailing changes introduced by temperature are limited to the changes in the gas properties present in all model equation. Instead, for powders of finer particles there is also a significant effect of temperature on the bed voidage that has to be taken into consideration. It is likely, that this effect is determined by an increase of interparticle forces that allow the stability of looser beds of particles.

Furthermore, the experimental bed expansion curves reveal the greatest tendency to expand for beds made of the finest samples at

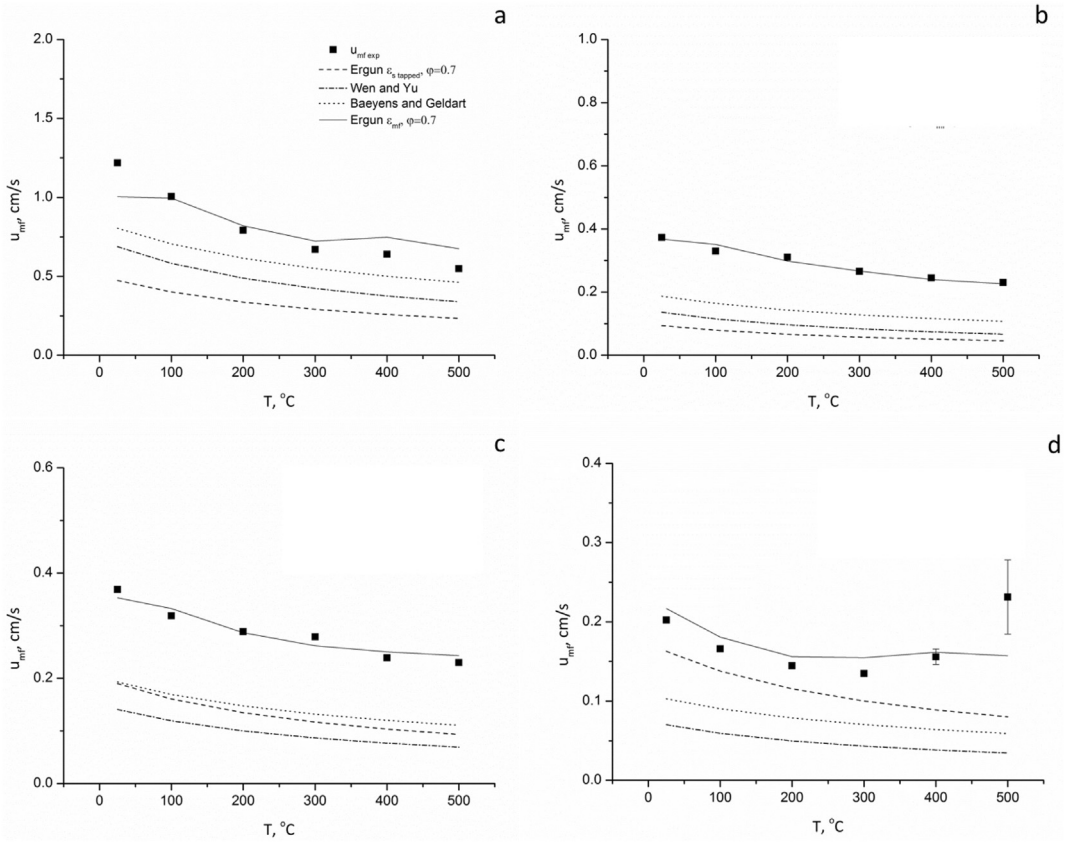

Fig. 24. Comparison between experimental and predicted u_{mf} values with increasing temperature using Eqs. (1)–(3): a) sample A5; b) sample A4; c) sample A3; d) sample A2.

Table 5
Averaged Relative errors for the different equations used to predict the Minimum fluidization velocity.

Material	A5	A4	A3	A2
Ergun, $\varphi = 0.7\ \varepsilon_{mf}$	59%	78%	54%	47%
Bayens and Geldart	24%	52%	50%	80%
Wen and Yu	40%	68%	66%	89%
Ergun, $\varphi = 0.7\ \varepsilon_s$	11%	3%	4%	11%

high temperatures. Moreover, voidages of the settled bed and at the minimum for fluidization were found to increase with temperature. Correspondingly to what has been observed with concern of fluidization pressure drops, bed expansion curves of systems made of A3 and A2 samples show important hysteresis phenomena. In particular, the higher height of the bed in the defluidizing branch of the expansion curve compared with the one in fluidizing branch at equal gas velocity, is due to changes the structure of the bed between the fluidization and the defluidization experiment, that lead to looser bed in this latter experiment. In fact, as the average particle size decreases, larger interparticle interactions stabilize the interparticle connections and result in a larger resistance of the particle bed to compact under its own weight. A similar behaviour was found by LaMarche et al. [65] in their experiments in presence of high air relative humidity, a situation that in a different way promotes the increase of the interparticle forces.

It was demonstrated that the bed expansion profiles plotted in the Richardson-Zaki form allowed to find best fitting values of n^* and u_t^* and that these values are quite different from n and u_t evaluated by using the Richardson-Zaki correlations and the theoretical values of the terminal Reynolds number calculated applying the Stokes drag. In the case of n^*, not only the values are different from n but also the trend with temperature is not the same of that found for n. Therefore, both the effect of temperature and of the particle size are quite different than those observed on the other parameters considered above like u_{mf} and ε_{mf}. This finding suggests that, in this case the discrepancies between experiment and calculations might not be exclusively attributed to the onset of interparticle forces, but perhaps also to the forced extension to homogeneous gas fluidization of the Richardson-Zaki correlations that were properly derived for liquids as fluidizing media.

5. Conclusions

A complete experimental characterization of the fluidization behaviour of powder samples of different particle sizes has been performed and some key conclusions can be drawn.

The results show that the mean size distribution affects significantly the fluidization behaviour of the materials investigated. In particular, significant differences were observed in the fluidization behaviour of the coarsest samples A5 and A4 and the finest sample A3 and A2. Sample A1, which exhibits the highest cohesive character, was impossible to be fluidized with an ordinary fluidized bed reactor.

For all materials tested, the fluidization curves provided the very first indication of the influence of the HDFs and IPFs on the fluidization behaviour. In fact, the measured pressure drops across the bed at full fluidization was within 1 or 2% of the theoretical value for gas suspensions for all the tested materials, indicating that the bed material was relatively free from any dominant effect of the interparticle forces in well fluidized conditions. Larger values of the pressure drop peak observed in the fluidization branch of the pressure drop profiles with the increasing operating temperature, highlights the role of temperature on the IPFs within the bed reactor. However, this result cannot be explained only by considering an increase of interparticle forces. Consistently, hysteresis phenomena were observed in the fluidization and defluidization branches of the fluidization curves obtained for the finest fluidizable samples (A3 and A2) and with increasing temperature. Different structures within the bed were detected with the X-ray images. In fact, the X-ray images enabled to identify the occurrence of channelling conditions. In this case it was possible to identify vertical or, in the case of the finest powder tested (A1) that could not be properly fluidized, horizontal channels in the bed.

Results suggest for fine particles a dominant role of IPFs over the HDFs when increasing temperature. The non-monotonic trend of u_{mf} with increasing temperature and consequent increase of u_{mf} for temperature higher than 300 °C cannot be explained only with the effects of temperature on the bed fluid dynamics, because both ε_{mf} and ε_s increase with temperature. Furthermore, the experimental expansion curves revealed a greatest tendency to expand for beds made of the finest samples at high temperatures.

The parameters of the Richardson-Zaki equation found with a fitting procedure on the experiments were found to be significantly different than the theoretical ones, predicted using the Richardson-Zaki correlations and the theoretical terminal velocity. Some of the experimental trends for the finest materials can be explained considering an active contribution of the IPFs in the particle systems, but the discrepancies between the fitting parameters and the model values perhaps should be attributed to breach of some model hypothesis.

Nomenclature

Acronyms

TGA	Thermogravimetric analysis –
DTA	Differential thermal analysis –
SEM	scanning electron microscope –
EDX	Energy Dispersive X-ray Analysis –

Symbols

A_c	cross-sectional area m^2
d_{43}	volume weighted mean particle size μm
d_{50}	size in correspondence of the 50th of the PSD μm
d_{90}	size in correspondence of the 90th of the PSD μm
d_{fd}	fluid dynamic particle diameter μm
d_{sv}	Sauter mean diameter of the PSD μm
g	Standard acceleration due to gravity μm
Ga	dimensionless Galileo number –
H	Height of the bed particle m
M	Mass of the bed material kg
n	Richardson and Zaki index –
n^*	Experimental Richardson and Zaki index –
p_f	particle compressive strength Pa
Re_t	dimensionless Reynolds number –
u_{mf}	Minimum fluidization velocity cm/s
u_t	terminal velocity of a single particle cm/s
u_t^*	Experimental terminal velocity of a single particle cm/s

Greek symbols

ΔP_c	Theoretical value of the pressure drops for bed fluidization Pa
ΔP_m	experimental value of the pressure drops across the bed μm
ε	porosity of the powder –
$\varepsilon_{changing\ slope}$	values of the voidage at the slope changes deg
ε_{mf}	Bed voidage at minimum fluidization condition –
ε_s	settled bed voidage –
μ	Gas viscosity Kg/m·s
ρ_{mix}	Density of the mixture kg/m^3
ρ_p	Particle density kg/m^3
ρ_g	Gas density kg/m^3
ψ	Particle shape factor –
φ	angle of internal friction deg

Supplementary data to this article can be found online at https://doi.org/10.1016/j.powtec.2019.11.102.

Acknowledgements

Authors are grateful for the financial support provided by our industrial partner and wish to thank Mr. Luciano Cortese of the IRC-CNR in Naples for his contribution in providing high quality SEM analyses.

References

[1] D. Kunii, O. Levenspiel, Fluidization Engineering, Butterworth-Heinemann, 1991.
[2] O. Molerus, Interpretation of Geldart's type A, B, C and D powders by taking into account interparticle cohesion forces, Powder Technol. 33 (1) (1982) 81–87, https://doi.org/10.1016/0032-5910(82)85041-9.
[3] D. Geldart, Types of gas fluidization, Powder Technol. 7 (5) (1973) 285–292, https://doi.org/10.1016/0032-5910(73)80037-3.
[4] P. Lettieri, J.G. Yates, D. Newton, The influence of interparticle forces on the fluidization behaviour of some industrial materials at high temperature, Powder Technol. 110 (1–2) (2000) 117–127, https://doi.org/10.1016/S0032-5910(99)00274-0.
[5] R. Chirone, L. Massimilla, S. Russo, Bubble-free fluidization of a cohesive powder in an acoustic field, Chem. Eng. Sci. 48 (1) (1993) 41–52, https://doi.org/10.1016/0009-2509(93)80281-T.
[6] P. Lettieri, D. Newton, J.G. Yates, High temperature effects on the dense phase properties of gas fluidized beds, Powder Technol. 120 (1–2) (2001) 34–40, https://doi.org/10.1016/S0032-5910(01)00344-8.
[7] R. Girimonte, B. Formisani, The minimum bubbling velocity of fluidized beds operating at high temperature, Powder Technol. 189 (1) (2009) 74–81, https://doi.org/10.1016/j.powtec.2008.06.006.
[8] J.G. Yates, Effects of temperature and pressure on gas-solid fluidization, Chem. Eng. Sci. 51 (2) (1996) 168–205.
[9] M.A.S. Quintanilla, J.M. Valverde, A. Castellanos, Adhesion force between fine particles with controlled surface properties, AICHE J. 52 (5) (2006) 1715–1728, https://doi.org/10.1002/aic.10770.
[10] J.M. Valverde, A. Castellanos, P. Mills, M.A.S. Quintanilla, Effect of particle size and interparticle force on the fluidization behavior of gas-fluidized beds, Phys. Rev. E 67 (5) (2003), 051305. https://doi.org/10.1103/PhysRevE.67.051305.
[11] S.M.P. Mutsers, K. Rietema, The effect of interparticle forces on the expansion of a homogeneous gas-fluidized bed, Powder Technol. 18 (2) (1977) 239–248, https://doi.org/10.1016/0032-5910(77)80014-4.
[12] K. Rietema, H.W. Piepers, The effect of interparticle forces on the stability of gas-fluidized beds – I. experimental evidence, Chem. Eng. Sci. 45 (6) (1990) 1627–1639.
[13] Q.F. Hou, Z.Y. Zhou, A.B. Yu, Micromechanical modeling and analysis of different flow regimes in gas fluidization, Chem. Eng. Sci. 84 (2012) 449–468.
[14] G. Donsì, L. Massimilla, Bubble-free expansion of gas-fluidized beds of fine particles, Bubble-Free Expansion of Gas-Fluidized Beds of Fine Particles, 19, 1973, pp. 41–53, https://doi.org/10.1002/aic.690190604.
[15] L. Massimilla, G. Donsì, C. Zucchini, The structure of bubble-free gas fluidized beds of fine fluid cracking catalyst particles, Chem. Eng. Sci. 27 (11) (1972) 2005–2015, https://doi.org/10.1016/0009-2509(72)87059-3.
[16] P. Lettieri, D. Macrì, Effect of process conditions on fluidization, KONA Powder Part J. 33 (October) (2016) 86–108, https://doi.org/10.14356/kona.2016017.
[17] N.S. Grewal, A. Gupta, Total and gas convective heat transfer from a vertical tube to a mixed particle gas-solid fluidized bed, Powder Technol. 57 (1989) 27–38.
[18] D. Geldart, Estimation of basic particle properties for use in fluid-particle process calculations, Powder Technol. 60 (1990) 1–13.
[19] J. Fletcher, M. Deo, F. Hanson, Re-examination of minimum fluidization velocity correlations applied to Group B sands and coked sands, Powder Technol. 69 (1992) 147–155.
[20] T.M. Knowlton, Pressure and temperature effects in fluid-particle systems, Pressure and Temperature Effects in Fluid-Particle Systems 1992, pp. 27–46.
[21] P. Lettieri, D. Newton, J.G. Yates, Homogeneous bed expansion of FCC catalysts, influence of temperature on the parameters of the Richardson–Zaki equation, Powder Technol. 123 (2–3) (2002) 221–231, https://doi.org/10.1016/S0032-5910(01)00463-6.
[22] R. Coltters, A.L. Rivas, Minimum fluidization velocity correlations in particulate systems, Powder Technol. 147 (2004) 34–48.
[23] B. Formisani, R. Girimonte, L. Mancuso, Analysis of the fluidization process of particle beds at high temperature, Chem. Eng. Sci. 53 (5) (1998) 951–961.
[24] J.H. Siegell, Early studies of magnetized-fluidized beds, Powder Technol. 57 (3) (1989) 213–220, https://doi.org/10.1016/0032-5910(89)80077-4.
[25] H. Piepers, E. Cottaar, A. Verkooijen, K. Rietema, Effects of pressure and type of gas on particle-particle interaction and the consequences for gas—solid fluidization behaviour, Powder Technol. 37 (1984) 55–70.
[26] E. Cottaar, K. Rietema, A theoretical study on the influence of gas adsorption on interparticle forces in powders, J. Colloid Interface Sci. 109 (1) (1986) 249–260.
[27] K. Rietema, E. Cottaar, H. Piepers, The effects of interparticle forces on the stability of gas-fluidized beds—II. Theoretical derivation of bed elasticity on the basis of van der Waals forces between, Chem. Eng. Sci. 48 (9) (1993) 1687–1697.
[28] B. Formisani, R. Girimonte, G. Pataro, The influence of operating temperature on the dense phase properties of bubbling fluidized beds of solids, Powder Technol. 125 (2002) 28–38.
[29] D. Geldart, A.C.Y. Wong, Fluidization of powders showing degrees of cohesiveness—II. Experiments on rates of de-aeration, Chem. Eng. Sci. 40 (1985) 653–661.
[30] C.L. Lin, M.Y. Wey, S.D. You, The effect of particle size distribution on minimum fluidization velocity at high temperature, Powder Technol. 126 (2002) 297–301.
[31] T. Zhou, H. Li, Estimation of agglomerate size for cohesive particles during fluidization, Powder Technol. 101 (1) (1999) 57–62, https://doi.org/10.1016/S0032-5910(98)00148-X.
[32] J.A. Agbim, A.W. Nienow, P.N. Rowe, Inter-particle forces that suppress bubbling in gas fluidised beds, Chem. Eng. Sci. 26 (1971) 1293–1294, https://doi.org/10.1016/0009-2509(71)87015-X.
[33] R. Chirone, D. Barletta, P. Lettieri, M. Poletto, Bulk flow properties of sieved samples of a ceramic powder at ambient and high temperature, Powder Technol. 288 (2016) 379–387, https://doi.org/10.1016/j.powtec.2015.11.040.
[34] P. Lettieri, J.G. Yates, New generation X-ray imaging for multiphase systems, Fluid XIV (2013) 641–648.
[35] J. Baeyens, D. Geldart, An investigation into slugging fluidized beds, Chem. Eng. Sci. 29 (1) (1974) 255–265, https://doi.org/10.1016/0009-2509(74)85051-7.
[36] C.Y. Wen, Y.H. Yu, A generalized method for predicting the minimum fluidization velocity, AICHE J. 12 (1966) 610–612.
[37] R.M. Nedderman, Cambridge University Press, Statics and Kinematics of Granular Materials, Cambridge University Press, 1992.
[38] D. Schulze, in: Springer Science & Business Media (Ed.), Powders and Bulk Solids, Springer Berlin Heidelberg, Berlin, Heidelberg, 2008 https://doi.org/10.1007/978-3-540-73768-1.
[39] ASTM International, ASTM D6773–02, Standard Shear Test Method for Bulk Solids Using the Schulze Ring Shear Tester, ASTM International, West Conshohocken, PA, 2008 https://doi.org/10.1520/D6682-08.
[40] M. Peleg, M.D. Normand, M.G. Corradini, Interactive software for calculating the principal stresses of compacted cohesive powders with the Warren-Spring equation, Powder Technol. 197 (3) (2010) 268–273, https://doi.org/10.1016/j.powtec.2009.10.003.
[41] J. Schwedes, Review on testers for measuring flow properties of bulk solids, Granul. Matter 5 (1) (2003) 1–43, https://doi.org/10.1007/s10035-002-0124-4.
[42] M.D. Ashton, D.C.H. Cheng, R. Farley, F.H.H. Valentin, Some investigations into the strength and flow properties of powders, Rheol. Acta 4 (3) (1965) 206–218, https://doi.org/10.1007/BF01969257.
[43] P. Pierrat, D.K. Agrawal, H.S. Caram, Effect of moisture on the yield locus of granular materials: theory of shift, Powder Technol. 99 (3) (1998) 220–227, https://doi.org/10.1016/S0032-5910(98)00111-9.
[44] H. Kamiya, A. Kimura, T. Yokoyama, M. Naito, G. Jimbo, Development of a split-type tensile-strength tester and analysis of mechanism of increase of adhesion behavior of inorganic fine powder bed at high-temperature conditions, Powder Technol. 127 (3) (2002) 239–245, https://doi.org/10.1016/S0032-5910(02)00117-1.
[45] A. Castellanos, J.M. Valverde, M.A.S. Quintanilla, The Sevilla powder tester: a tool for characterizing the physical properties of fine cohesive powders at very small consolidations, KONA Powder Part J. 22 (22) (2004) 66–81, https://doi.org/10.14356/kona.2004011.
[46] U. Zafar, C. Hare, G. Calvert, et al., Comparison of cohesive powder flowability measured by Schulze shear cell, raining bed method, Sevilla powder tester and new ball indentation method, Powder Technol. 286 (2015) 807–816, https://doi.org/10.1016/j.powtec.2015.09.010.
[47] H. Rumpf, ZurTheorie der Zugfestigkeit von Agglomeratenbei Kraftübertragungan Kontaktpunkten, Chem. Ing. Tech. 42 (1970) 538–540.
[48] O. Molerus, Theory of yield of cohesive powders, Powder Technol. 12 (3) (1975) 259–275, https://doi.org/10.1016/0032-5910(75)85025-X.
[49] I. Tomasetta, D. Barletta, M. Poletto, Correlation of powder flow properties to interparticle interactions at ambient and high temperatures, Particuology 12 (1) (2014) 90–99, https://doi.org/10.1016/j.partic.2013.02.002.
[50] R. Chirone, F. Raganati, P. Ammendola, D. Barletta, P. Lettieri, M. Poletto, A comparison between interparticle forces estimated with direct powder shear testing and with sound assisted fluidization, Powder Technol. 323 (2018) 1–7, https://doi.org/10.1016/j.powtec.2017.09.038.
[51] R. Chirone, D. Barletta, M. Poletto, P. Lettieri, Detection and estimation of capillary interparticle forces in the material of a fluidized bed reactor at high temperature by powder flow characterization, Powder Technol. 330 (2018) 371–385, https://doi.org/10.1016/j.powtec.2018.02.024.
[52] D. Macrì, M. Poletto, D. Barletta, S. Sutcliffe, P. Lettieri, Analysis of industrial reactive powders flow properties at high temperature, Powder Technol. 316 (2017) 131–138, https://doi.org/10.1016/j.powtec.2016.10.064.
[53] D. Macrì, D. Barletta, P. Lettieri, M. Poletto, Experimental and theoretical analysis of TiO2 powders flow properties at ambient and high temperatures, Chem. Eng. Sci. 167 (2017) 172–190, https://doi.org/10.1016/j.ces.2017.03.057.
[54] Y. Liu, H. Lu, D. Barletta, et al., Bulk flow properties of fly ashes at ambient and high temperature, Particuology 38 (2018) 113–125, https://doi.org/10.1016/j.partic.2017.04.013.
[55] Y. Liu, H. Lu, M. Poletto, X. Guo, X. Gong, Y. Jin, Flow properties and inter-particle forces in fuel powders, Particuology 34 (2017) https://doi.org/10.1016/j.partic.2016.10.007.
[56] D. Sofia, D. Barletta, M. Poletto, Laser sintering process of ceramic powders: the effect of particle size on the mechanical properties of sintered layers, Addit. Manuf. 23 (2018) 215–224, https://doi.org/10.1016/j.addma.2018.08.012.

[57] D. Sofia, R. Chirone, P. Lettieri, D. Barletta, M. Poletto, Selective laser sintering of ceramic powders with bimodal particle size distribution, Chem. Eng. Res. Des. 136 (2018) 536–547, https://doi.org/10.1016/j.cherd.2018.06.008.
[58] D. Barletta, G. Donsi, G. Ferrari, et al., Solid flow rate prediction in silo discharge of aerated cohesive powders, AICHE J. 53 (9) (2007) 2240–2253, https://doi.org/10.1002/aic.11212.
[59] D. Barletta, M. Poletto, Aggregation phenomena in fluidization of cohesive powders assisted by mechanical vibrations, Powder Technol. 225 (2012) 93–100, https://doi.org/10.1016/j.powtec.2012.03.038.
[60] V. Domnich, Y. Aratyn, W.M. Kriven, Y. Gogotsi, Temperature dependence of silicon hardness: experimental evidence of phase transformations, Rev. Adv. Mater. Sci. 17 (1–2) (2008) 33–41.
[61] W.N. Zaki, J.F. Richardson, Sedimentation and fluidisation: part I, Trans. Inst. Chem. Eng. 32 (1954) 35–53.
[62] C. Zhu, Q. Yu, R. Dave, R. Pfeffer, Gas fluidization characteristics of nanoparticle agglomerates, AICHE J. 51 (2) (2005) 426–439.
[63] P.N. Loezos, P. Costamagna, S. Sundaresan, The role of contact stresses and wall friction on fluidization, Chem. Eng. Sci. (2002) https://doi.org/10.1016/S0009-2509(02)00421-9.
[64] S.C. Tsinontides, R. Jackson, The mechanics of gas fluidized beds with an interval of stable fluidization, J. Fluid Mech. 255 (1) (1993) 237, https://doi.org/10.1017/S0022112093002472.
[65] C.Q. LaMarche, A.W. Miller, P. Liu, C.M. Hrenya, Linking micro-scale predictions of capillary forces to macro-scale fluidization experiments in humid environments, AICHE J. 62 (10) (2016) 3585–3597, https://doi.org/10.1002/aic.15281.